A double-faced 6R Single-loop Overconstrained Spatial Mechanism*

Xianwen Kong
School of Engineering and Physical Sciences, Heriot-Watt University
Edinburgh, UK, EH14 4AS
email: X.Kong@hw.ac.uk

Xiuyun He
School of Engineering and Physical Sciences, Heriot-Watt University
Edinburgh, UK, EH14 4AS
email: xiuyunhe@gmail.com

Duanling Li
Automation School
Beijing University of Posts and Telecommunications
Beijing 100876, China
email: liduanling@163.com

ABSTRACT

This paper deals with a 6R single-loop overconstrained spatial mechanism that has two pairs of revolute joints with intersecting axes and one pair of revolute joints with parallel axes. The 6R mechanism is first constructed from an isosceles triangle and a pair of identical circles. The kinematic analysis of the 6R mechanism is then dealt with using a dual quaternion approach. The analysis shows that the 6R mechanism usually has two solutions to the kinematic analysis for a given input and may have two circuits (closure modes or branches) with one or two pairs of full-turn revolute joints. In two configurations in each circuit of the 6R mechanism, the axes of four revolute joints are coplanar, and the axes of the other two revolute joints are perpendicular to the plane defined by the above four revolute joints. Considering that from one configuration of the 6R mechanism, one can obtain another configuration of the mechanism by simply renumbering the joints, the concept of two-faced mechanism is introduced. The formulas for the analysis of plane symmetric spatial triangle is also presented in this paper. These formulas will be useful for the design and analysis of multi-loop overconstrained mechanisms involving plane symmetric spatial RRR triads.

KEY WORDS Overconstrained Mechanism, Geometric Approach, Dual Quaternion, Two-faced Mechanism, Plane Symmetric Spatial Triangle

1 Introduction

Fruitful results have been obtained in the past decades in the research on single degree-of-freedom (DOF) single-loop overconstrained mechanisms [1–26]. Although the successful industrial applications of single-loop overconstrained mechanisms are quite limited, single-loop overconstrained mechanisms are being used in the development of parallel mechanisms [27, 28], deployable structures [13, 29], mobile robots [30], multi-mode mechanisms [31–37] and other devices [38].

The methods for obtaining 6R mechanisms mainly include: geometric methods [1, 23, 26], construction approaches [3, 4, 6, 13, 22], algebraic approaches [7, 11, 14–16, 19–21, 25, 39] and numerical methods [8]. For a comprehensive list of 6R mechanisms, refer to [14, 17, 25, 26]. Like in the type synthesis of translational parallel mechanisms or the analysis of slide-crank mechanism [40], several earlier work on 6R mechanisms, such as [9, 24], have also been unfortunately ignored for decades. In addition, several 6R mechanisms can be obtained using different approaches.

Searching for 6R mechanisms is still not fully solved. For example, 6R mechanisms that have either three pairs of revolute (R) joints with intersecting axes [26] or three pairs of R joints with parallel axes [19, 22, 23] have been identified. It is logical to identify 6R mechanisms that have two pairs of R joints with intersecting axes and one pair of R joints with parallel axes. However, only one such mechanism, the Schatz's 6R mechanism, has been presented so far. It is unclear

*The original version of this paper was presented at the ASME 2017 International Design Engineering Technical Conferences & Computers and Information in Engineering Conference, DETC2017-67419, August 7–9, 2017, Cleveland, Ohio, USA

whether there are any other 6R mechanisms that have two pairs of R joints with intersecting axes and one pair of R joints with parallel axes.

Inspired by the geometric construction of Bricard 6R mechanisms [1,2] and the 6R mechanism that has three pairs of R joints with intersecting axes [26], this paper aims at revealing a 6R mechanism that has two pairs of R joints with intersecting axes and one pair of R joints with parallel axes. The Bricard's trihedral 6R mechanism can be constructed from a triangle. In the configuration of construction, the axes of its three R joints are on the plane defined by the triangle and those of the remaining three R joints are perpendicular to the triangle. The Type III Bricard's mobile octahedral 6R mechanism can be constructed from a triangle with two concentric circles. In the configuration of construction, the axes of all the six R joints are on the plane defined by the triangle. In [26], a 6R mechanism that has three pairs of R joints with intersecting axes is constructed from a kite and a pair of identical circles.

This paper is organized as follows. A 6R mechanism that has two pairs of R joints with intersecting axes and one pair of R joints with parallel axes will be constructed from an isosceles triangle and a pair of circles in Section 2. The kinematic analysis of the 6R mechanism using a dual quaternion based approach will be presented in Section 3, where two example 6R mechanisms with different number of full-turn R joints are given. In Section 4, the characteristics of the 6R mechanism will be revealed and the concept of two-faced mechanism will be introduced. Finally, conclusions are drawn.

For simplicity reasons, $\sin\theta_i$ and $\cos\theta_i$ are denoted by $S\theta_i$ and $C\theta_i$, respectively.

2 Description of a 6R mechanism that has two pairs of R joints with intersecting axes and one pair of R joints with parallel axes

In this section, a 6R mechanism will be constructed from an isosceles triangle and a pair of identical circles. In the configuration of construction, the axes of four R joints are on the plane determined by the triangle, while those of the remaining two R joints are perpendicular to the triangle. The geometric construction of the 6R mechanism will be presented first. The D-H (Denavit-Hartenberg) link parameters of the 6R mechanism will then be given.

2.1 Geometric construction of a 6R mechanism

A 6R mechanism can be constructed as follows (Fig. 1):

Step 1: Draw six lines for placing R (revolute) joints [Fig. 1(a)].
At first, draw (a) an isosceles triangle ABC where $|AC| = |BC|$, (b) one altitude CC' of triangle ABC, and (c) two identical circles of radius r ($r \leq |AC| = |BC|$) with their centers at A and B respectively. Then, draw (a) lines AA' and BB' that are perpendicular to the triangle ABC, (b) lines $A_1A'_1$ and $B_1B'_1$ on the same side of line CC' that are tangent to circles A and B at points A and B respectively, and (c) lines CA_2 and CB_2 that are tangent to circles A and B respectively at points A_2 and B_2 such that tangent points A_1 and A_2 are on two sides of line AC and tangent points B_1 and B_2 are on two sides of line BC. Lines $A_1A'_1$, AA', CA_2, $B_1B'_1$, BB', and CB_2 are the six lines required for placing six R joints.

Step 2: Construct a 6R mechanism using the six lines obtained in Step 1 [Fig. 1(b)].
Place six R joints 1, 2, $\cdots$, 6 along lines $A_1A'_1$, AA', CA_2, CB_2, BB', and $B_1B'_1$ respectively and connect them in the sequence of 1-2-3-4-5-6-1. One then obtains a 6R mechanism 1-2-3-4-5-6-1.

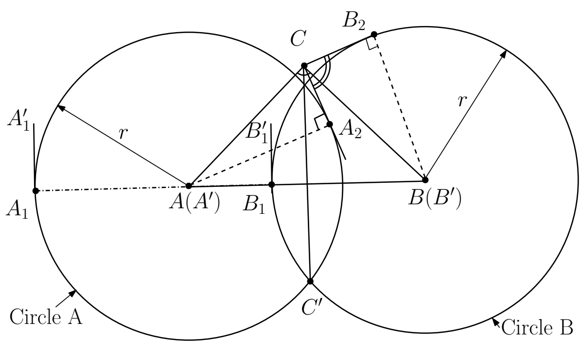

(a) Step 1.

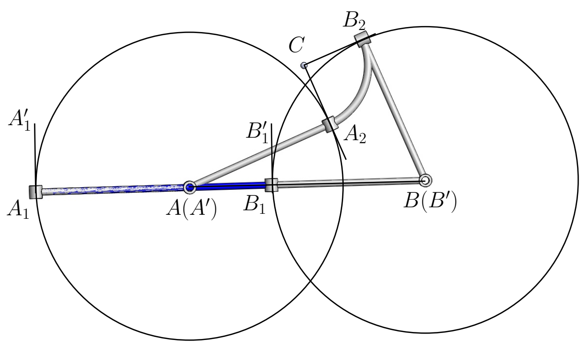

(b) Step 2.

Fig. 1. Construction of a 6R mechanism that has two pairs of R joints with intersecting axes and one pair of R joints with parallel axes.

It is noted that $\angle ACB = \angle A_2CB_2$, $|CA_2| = |CB_2|$, $|A_1B_1| = |AB|$. Therefore

$$|A_1B_1| = |AB| = 2\sqrt{|CA_2|^2 + r^2}S(\angle A_2CB_2/2) \tag{1}$$

2.2 Link parameters of the 6R mechanism

For clarity, the frame, link 6 connecting joints 6 and 1, of the 6R mechanism will be highlighted in blue throughout this paper.

As in [26], coordinate frames in the 6R mechanism are attached to the links as follows (Fig. 2): Z_i-axis is along the axis of joint i. X_i-axis is along the common perpendicular between Z_{i-1}- and Z_i-axes. O_i is the intersection of X_i- and Z_i-axes. Y_i-axis is defined by X_i- and Z_i-axes through the right handed rule and omitted in Fig. 2. The joint variable, θ_i, is defined as the angle between X_i- and X_{i+1}-axes measured from X_i-axis to X_{i+1}-axis about Z_i-axis. The link parameters of link i are:

d_i: Distance between X_i- and X_{i+1}-axes measured from X_i-axis to X_{i+1}-axis along Z_i-axis
α_i: Twist angle between Z_i- and Z_{i+1} axes measured from Z_i-axis to Z_{i+1}-axis about X_{i+1}-axis
l_i: Distance between Z_i- and Z_{i+1}-axes measured from Z_i-axis to Z_{i+1}-axis along X_{i+1}-axis

.

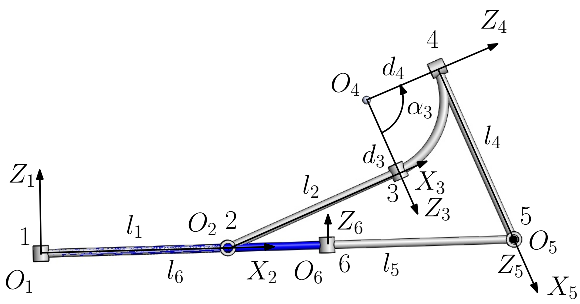

Fig. 2. D-H parameters of the 6R mechanism.

The link parameters of the 6R mechanism are:
$d_2 = d_5 = 0$, $d_6 = -d_1$, $d_4 = -d_3$,
$\alpha_1 = \alpha_2 = \alpha_4 = \alpha_5 = \pi/2$, $\alpha_6 = 0$, α_3,
$l_3 = 0$, $l_1 = l_2 = l_4 = l_5$, and l_6.

From Fig. 1 and Eq. (1), we learn that the link parameters of the 6R mechanism satisfy:

$$l_6 = 2\sqrt{d_3^2 + l_1^2}S(\alpha_3/2) \tag{2}$$

2.3 The 6R mechanism as a special case of Wohlhart's double-Goldberg-5R 6R mechanism

In this section, we will show that the proposed 6R mechanism is in fact a special case of the Wohlhart's double-Goldberg-5R 6R mechanism [6].

2.3.1 Construction of Wohlhart's double-Goldberg-5R 6R mechanism

A Wohlhart's double-Goldberg-5R 6R mechanism 1-2-3-4-5-6 [Fig. 3(a)] is obtained by merging two Goldberg 5R mechanisms that have two common links, 1-2-8-5-6 and 2-3-4-5-8 [Fig. 3(b)], and then removing the two common links. Each Goldberg 5R mechanism 2-3-4-5-8 is obtained by merging two Bennett linkages [Fig. 3(c)] sharing a common link, 2-3-9-8 and 9-4-5-8, removing the common link 8-9 and locking the angle between two links 3-9 and 9-4 adjacent to the common link. All the links in the associated Bennett linkages [Fig. 3(c)] have the same Bennett ratio and fall into four groups of links with identical link parameters: 2-3, 8-9 and 5-4; 1-2, 7-8 and 6-5; 7-1, 8-2 and 9-3; 6-7, 5-8 and 4-9.

2.3.2 A plane symmetric spatial triangle

Calculating the link parameters of a Goldberg-5R mechanism requires the analysis of a spatial triangle. The analysis of a general spatial triangle has been presented in the literature (see [41] for example). Here the analysis of a plane symmetric spatial triangle (Fig. 4) will be discussed. In the plane symmetric spatial triangle, the axes of R joints 2 and 3 are symmetric

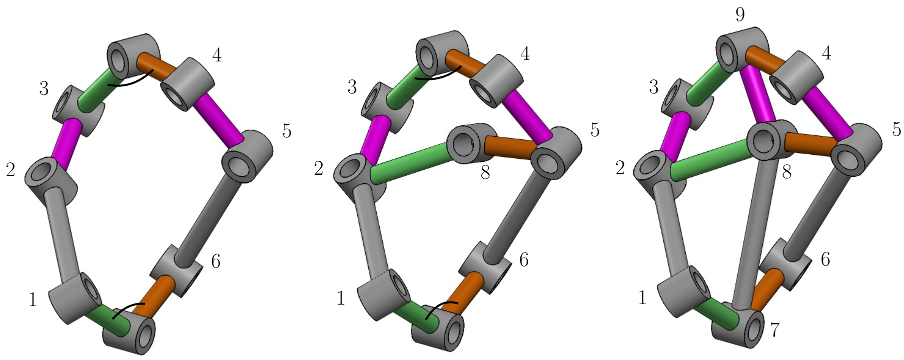

(a) Wohlhart's 6R mechanism. (b) Two compositional Goldberg 5R mechanisms. (c) Bennett's linkages associated with Goldberg 5R mechanisms.

Fig. 3. Wohlhart's double-Goldberg-5R 6R mechanism.

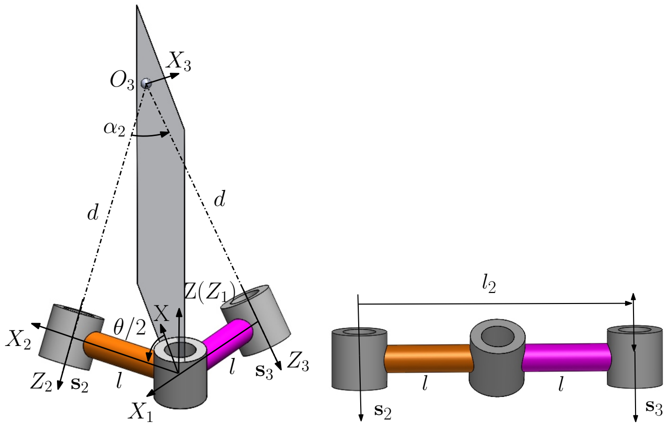

(a) General case. (b) Degenerate case.

Fig. 4. A plane symmetric spatial triangle.

about a plane passing through the axis of R joint 1. Let Z-axis coincide with Z_1-axis and X-axis be located on the plane of symmetry. For brevity, the twist angle between the axes of R joints 1 and 2 is denoted by α, and the joint variable of R joint 1 is denoted by θ.

Since point O_3 is on the plane of symmetry, we have

$$-dC(\theta/2)S\alpha + lS(\theta/2) = 0 \tag{3}$$

In addition, $\mathbf{s}_2 = \{S(\theta/2)S\alpha \quad -C(\theta/2)S\alpha \quad C\alpha\}^T$ and $\mathbf{s}_3 = \{S(\theta/2)S\alpha \quad C(\theta/2)S\alpha \quad C\alpha\}^T$. Then

$$\mathbf{s}_2 \cdot \mathbf{s}_3 = S^2(\theta/2)S^2\alpha - C^2(\theta/2)S^2\alpha + C^2\alpha = C\alpha_2 \tag{4}$$

Equation (4) can be turned into the following form

$$S^2(\theta/2)S^2\alpha - C^2(\theta/2)S^2\alpha + (1 - S^2\alpha) = 1 - 2S^2(\alpha_2/2)$$

and then simplified as

$$C^2(\theta/2)S^2\alpha = S^2(\alpha_2/2) \tag{5}$$

Equations (3) and (5) lead to

$$l^2S^2(\theta/2) = d^2S^2(\alpha_2/2) \tag{6}$$

From Eqs. (5) and (6) together with $S^2(\theta/2)+C^2(\theta/2)=1$, we obtain

$$l^2S^2\alpha=(d^2S^2\alpha+l^2)S^2(\alpha_2/2) \tag{7}$$

i.e.,

$$l^2=(d^2+l^2/S^2\alpha)S^2(\alpha_2/2) \tag{8}$$

If the axes of R joints 2 and 3 are parallel, we have

$$l_2=2l \tag{9}$$

and

$$d=0 \tag{10}$$

2.3.3 A special case of Wohlhart's double-Goldberg-5R 6R mechanism

Now let us consider the following special case of the Wohlhart's double-Goldberg-5R 6R mechanism [Fig. 5(a)]. In its associated Bennett linkages [Fig. 5(c)], 2-3, 8-9, 5-4, 1-2, 7-8 and 6-5 are identical links with a twist angle of $\pi/2$. In addition, the axes of R joints 3 and 4 (2 and 5; 1 and 6) are symmetric about a plane passing through the axis of R joint 9 (8; 7). In addition, R joint 7 is locked when links 1-7 and 7-6 are collinear [Fig. 5(b)].

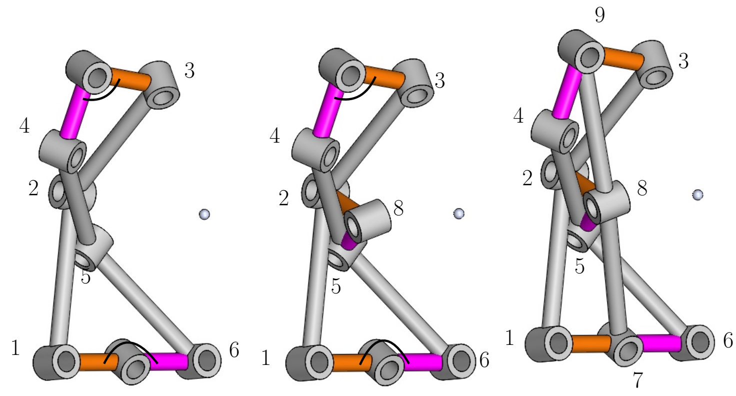

(a) Wohlhart's 6R mechanism. (b) Two compositional Goldberg 5R mechanisms. (c) Bennett's linkages associated with Goldberg 5R mechanisms.

Fig. 5. A special case of Wohlhart's double-Goldberg-5R 6R mechanism.

Using Eq. (8), we obtain from the spatial triangle composed of the axes of R joints 4, 9 and 3 (Figs. 5(c)and 2)

$$l^2=[d_3+l^2/S^2(\alpha/2)]S^2(\alpha_3/2) \tag{11}$$

Since all the links within the Bennett linkages associated with the Wohlhart's double-Goldberg-5R 6R mechanism has the same Bennett ratio, we have

$$l_1^2=l^2/S^2(\alpha/2) \tag{12}$$

Substitution of Eq. (12) into Eq. (11) yields

$$l^2=(d_3+l_1^2)S^2(\alpha_3/2) \tag{13}$$

Using Eq. (9), we obtain from the spatial triangle composed of the axes of R joints 1, 7 and 6 (Figs. 5(c) and 2)

$$l_6 = 2l \tag{14}$$

Equations (13) and (14) lead to

$$l_6^2 = 4(d_3^2 + l_1^2)S^2(\alpha_3/2) \tag{15}$$

Equations (15) and (2) are in fact identical. Therefore, the 6R mechanism constructed in Section 2.1 is a special case of the Wohlhart's double-Goldberg-5R 6R mechanism. However, it is more concise to obtain this 6R mechanism using the geometric construction method than the Goldberg 5R linkage based construction method.

3 Kinematic Analysis of the 6R mechanism

Although an approach to the kinematic analysis of Wohlhart's double-Goldberg-5R 6R mechanism has been given in [6], one needs to calculate the unknown link parameters of the Goldberg 5R mechanisms first. In this section, the kinematic analysis of the 6R mechanism using the dual quaternion based approach (see [25, 37] for example) will be presented. Using this approach, one does not need to calculate the unknown link parameters of the Goldberg 5R mechanisms. In addition, 6R mechanisms with different numbers of full-turn R joints will also be given.

The displacement of a link can be represented using a dual quaternion as[1]

$$Q = e_0 + e_1\mathbf{i} + e_2\mathbf{j} + e_3\mathbf{k} + \varepsilon(g_0 + g_1\mathbf{i} + g_2\mathbf{j} + g_3\mathbf{k}) \tag{16}$$

where $e_0 g_0 + e_1 g_1 + e_2 g_2 + e_3 g_3 = 0$.

The dual quaternions representing translation about X$_i$-axis by l_i, translation about Z$_i$-axis by d_i, rotation about X$_i$-axis by α_i, rotation about Z$_i$-axis by θ_i, and no motion are

$$Q_{TranX_i} = 1 + \varepsilon(l_i/2)\mathbf{i} \tag{17}$$

$$Q_{TranZ_i} = 1 + \varepsilon(d_i/2)\mathbf{k} \tag{18}$$

$$Q_{RotX_i} = C(\alpha_i/2) + S(\alpha_i/2)\mathbf{i} \tag{19}$$

$$\check{Q}_{RotZ_i} = t_i + \mathbf{k} \tag{20}$$

where $t_i = cot(\theta_i/2)$

$$Q_E = 1 \tag{21}$$

The product of two dual quaternions satisfies the following rules:

$$\begin{aligned}
&\mathbf{i}^2 = \mathbf{j}^2 = \mathbf{k}^2 = \mathbf{ijk} = -1 \\
&\mathbf{ij} = \mathbf{k} = -\mathbf{ji} \\
&\mathbf{jk} = \mathbf{i} = -\mathbf{kj} \\
&\mathbf{ki} = \mathbf{j} = -\mathbf{ik} \\
&\varepsilon^2 = 0 \ \text{ and } \ \varepsilon \neq 0
\end{aligned} \tag{22}$$

[1] There are several different notations for dual quaternions in the literature. For example, $g = a_0 + a_1 i + a_2 j + a_3 k + \varepsilon(c_0 + c_1 i + c_2 j + c_3 k)$ is used in [42].

A set of six equations in t_i ($i = 1, 2, \cdots 6$) for the 6R mechanism is [37]

$$\begin{cases} e_1(t_1, t_2, \cdots t_6) = 0 \\ e_2(t_1, t_2, \cdots t_6) = 0 \\ e_3(t_1, t_2, \cdots t_6) = 0 \\ g_1(t_1, t_2, \cdots t_6) = 0 \\ g_2(t_1, t_2, \cdots t_6) = 0 \\ g_3(t_1, t_2, \cdots t_6) = 0 \end{cases} \tag{23}$$

Equation (23) is in fact composed of the second, third, fourth, sixth, seventh and eighth scalar equations of Eq. (24).

$$\prod_{i=1}^{6} (\check{Q}_{RotZ_i} Q_{TranZ_i} Q_{TranX_i} Q_{RotX_i}) = Q_E / \prod_{i=1}^{6} S(\theta_i/2) \tag{24}$$

To exclude the extraneous solutions with $t_i = \pm I$ before solving Eq. (23) [25], one can introduce an extra variable v and add the equation $(t_1^2+1)(t_2^2+1)\cdots(t_6^2+1)v - 1 = 0$ to Eq. (23) and compute an elimination ideal that eliminates v with the software Maple to obtain a new set of equations. By calculating the Gröbner basis of the ideal spanned by this set of equations, one can obtain the input-output equation of the 6R mechanism.

3.1 Mechanism I: Mechanism with one pair of full-turn R joints

The link parameters of Mechanism I are:
$d_2 = d_5 = 0$, $d_6 = -d_1 = 0$, $d_4 = -d_3 = 10$
$\alpha_1 = \alpha_2 = \alpha_4 = \alpha_5 = \pi/2$, $\alpha_6 = 0$, $\alpha_3 = \pi/2$,
$l_3 = 0$, $l_1 = l_2 = l_4 = l_5 = 50$, and $l_6 = 50\sqrt{10}$.

Here, l_6 is calculated using Eq. (2).

In the following, the detailed kinematic analysis of Mechanism I will be presented.

Substituting the above link parameters into Eq. (24) and taking the second, third, fourth, sixth, seventh and eighth scalar equations, we obtain the specific form of Eq. (23) for Mechanism I as

$$\begin{cases} e_1(t_1, t_2, \cdots t_6) = -t_1t_2t_3t_4t_5t_6 - t_1t_2t_3t_4 - t_1t_2t_3t_5 - t_1t_2t_3t_6 \\ +t_1t_2t_4t_5 - t_1t_2t_4t_6 - t_1t_2t_5t_6 + t_1t_3t_4t_5 + t_1t_3t_4t_6 - t_1t_3t_5t_6 - t_1t_4t_5t_6 \\ -t_2t_3t_4t_5 + t_2t_3t_4t_6 + t_2t_3t_5t_6 - t_2t_4t_5t_6 - t_3t_4t_5t_6 + t_1t_2 - t_1t_3 + t_1t_4 - t_1t_5 \\ +t_1t_6 - t_2t_3 - t_2t_4 - t_2t_5 - t_2t_6 + t_3t_4 - t_3t_5 + t_3t_6 - t_4t_5 - t_4t_6 + t_5t_6 + 1 = 0 \\ e_2(t_1, t_2, \cdots t_6) = t_1t_2t_3t_4t_5 - t_1t_2t_3t_4t_6 - t_1t_2t_3t_5t_6 + t_1t_2t_4t_5t_6 \\ +t_1t_3t_4t_5t_6 - t_2t_3t_4t_5t_6 + t_1t_2t_3 + t_1t_2t_4 + t_1t_2t_5 + t_1t_2t_6 - t_1t_3t_4 + t_1t_3t_5 \\ -t_1t_3t_6 + t_1t_4t_5 + t_1t_4t_6 - t_1t_5t_6 - t_2t_3t_4 - t_2t_3t_5 - t_2t_3t_6 + t_2t_4t_5 - t_2t_4t_6 - t_2t_5t_6 \\ +t_3t_4t_5 + t_3t_4t_6 - t_3t_5t_6 - t_4t_5t_6 - t_1 + t_2 - t_3 + t_4 - t_5 + t_6 = 0 \\ \cdots \end{cases} \tag{25}$$

Eliminating the solutions with $t_i = \pm I$ to Eq. (25) by calculating the elimination ideal using the Maple command *EliminationIdeal*, one obtain the following set of 15 equations.

$$\begin{cases} 3t_1t_6 - 2\sqrt{10} + 7 = 0 \\ -2\sqrt{10}t_1t_2 - 7t_1t_2 + 3t_1t_5 + 3t_2t_3 - 5t_3t_5 + 4t_3 - 4t_5 + 2 = 0 \\ \cdots \\ 3t_2t_3 - 5t_2t_4 - 5t_3t_5 + 3t_4t_5 + 4t_2 + 4t_3 - 4t_4 - 4t_5 + 4 = 0 \end{cases} \tag{26}$$

Calculating the Gröbner basis of the ideal spanned by Eq. (26) using *Groebner:-Basis* in lexicographic order with $t_6 > t_5 > t_4 > t_3 > t_1 > t_2$, we obtain the input-output equation of Mechanism I as

$$\begin{gathered} 9t_1^2t_2^2 + \left(-12\sqrt{10} + 24\right)t_1^2t_2 + \left(-6\sqrt{10} + 21\right)t_1^2 + \\ \left(-28\sqrt{10} + 89\right)t_2^2 + \left(44\sqrt{10} - 136\right)t_2 - 6\sqrt{10} + 21 = 0 \end{gathered} \tag{27}$$

Substituting $t_i = (1 + C\theta_i)/S\theta_i$ $(i = 1, 2)$ into Eq. (27)[2] into Eq. (36) and simplifying the resulted equation, we obtain

$$\begin{aligned} &10C\theta_1 C\theta_2 - 20C\theta_1 S\theta_2 + 2\sqrt{10}C\theta_2 \\ &-4\sqrt{10}S\theta_2 + 10C\theta_1 + 5\sqrt{10} = 0 \end{aligned} \tag{28}$$

For a given set of θ_1 and θ_2, one can determine θ_i $(i = 3, 4, \cdots 6)$ by calculating $t_i = cot(\theta_i/2)$ using the following equations.

$$\begin{aligned} t_3 = -[&(-2\sqrt{10} - 7)t_1 t_2^2 + (4\sqrt{10} + 8)t_1 t_2 \\ &-3t_1 + 10t_2]/(3t_2^2 + 8t_2 - 3) \end{aligned} \tag{29}$$

$$t_4 = (2t_3 + 1)/(t_3 + 2) \tag{30}$$

$$t_5 = -(2t_2 + 1)/(t_2 - 2) \tag{31}$$

$$t_6 = (2\sqrt{10} - 7)/(3t_1) \tag{32}$$

The variation of θ_i $(i = 2, 3 \cdots 6)$ with θ_1 for Mechanism I is shown in Fig. 6. It is observed from Fig. 6 that Mechanism I has two circuits represented in solid and dashed lines respectively and joints 3 and 4 are full-turn R joints. Figures 7 and 8 show the 6R Mechanism I at configurations A, B and C in circuit 1 and configurations D, E and F in circuit 2 respectively. At two configurations in each circuit (see configurations A and C in circuit 1 and configurations D and F in circuit 2), the axes of R joints 1, 3, 4 and 6 are coplanar and the axes of R joints 2 and 5 are perpendicular to the plane defined by the axes of R joints 1, 3, 4 and 6.

From Eq. (28) and Fig. 6(a), we learn that to ensure θ_2 has real solutions requires $-2\pi \leq \theta_1 \leq -\theta_{1b}$, $-\theta_{1a} \leq \theta_1 \leq \theta_{1a}$, or $\theta_{1b} \leq \theta_1 \leq 2\pi$. Here $\theta_{1a} = arccos(-\sqrt{10}/8 + 3\sqrt{2}/8)$ and $\theta_{1b} = \pi - arccos(\sqrt{10}/8 + 3\sqrt{2}/8)$. When plotting the θ_6-θ_1 curve in Fig. 6(e) using Eq. (32), we must limit θ_1 to the above ranges.

Re-calculating the Gröbner basis of the ideal spanned by Eq. (26) using *Groebner:-Basis* in lexicographic order with $t_6 > t_5 > t_4 > t_2 > t_1 > t_3$, $t_6 > t_5 > t_3 > t_2 > t_1 > t_4$ and $t_6 > t_4 > t_3 > t_2 > t_1 > t_5$, we can derive the explicit input-output equations between θ_3 (θ_4 or θ_5) and θ_1 as

$$\begin{aligned} &3t_1^2 t_3^2 + (-4\sqrt{10} + 8)t_1 t_3^2 - 3t_1^2 + (-4\sqrt{10} + 8)t_1 t_3 \\ &+(-2\sqrt{10} + 7)t_3^2 + (-4\sqrt{10} + 8)t_1 + 2\sqrt{10} - 7 = 0 \end{aligned} \tag{33}$$

$$\begin{aligned} &3t_1^2 t_4^2 + (-4\sqrt{10} + 8)t_1 t_4^2 - 3t_1^2 + (4\sqrt{10} - 8)t_1 t_4 \\ &+(-2\sqrt{10} + 7)t_4^2 + (-4\sqrt{10} + 8)t_1 + 2\sqrt{10} - 7 = 0 \end{aligned} \tag{34}$$

$$\begin{aligned} &3t_1^2 t_5^2 + (-4\sqrt{10} - 8)t_1^2 t_5 + (2\sqrt{10} + 7)t_1^2 + 3t_5^2 \\ &+(4\sqrt{10} - 8)t_5 - 2\sqrt{10} + 7 = 0 \end{aligned} \tag{35}$$

[2]For some polynomial equations, we need to use $t_i = C(\theta_i/2)/S(\theta_i/2)$ in order to avoid extraneous curve $\theta_i = \pi$.

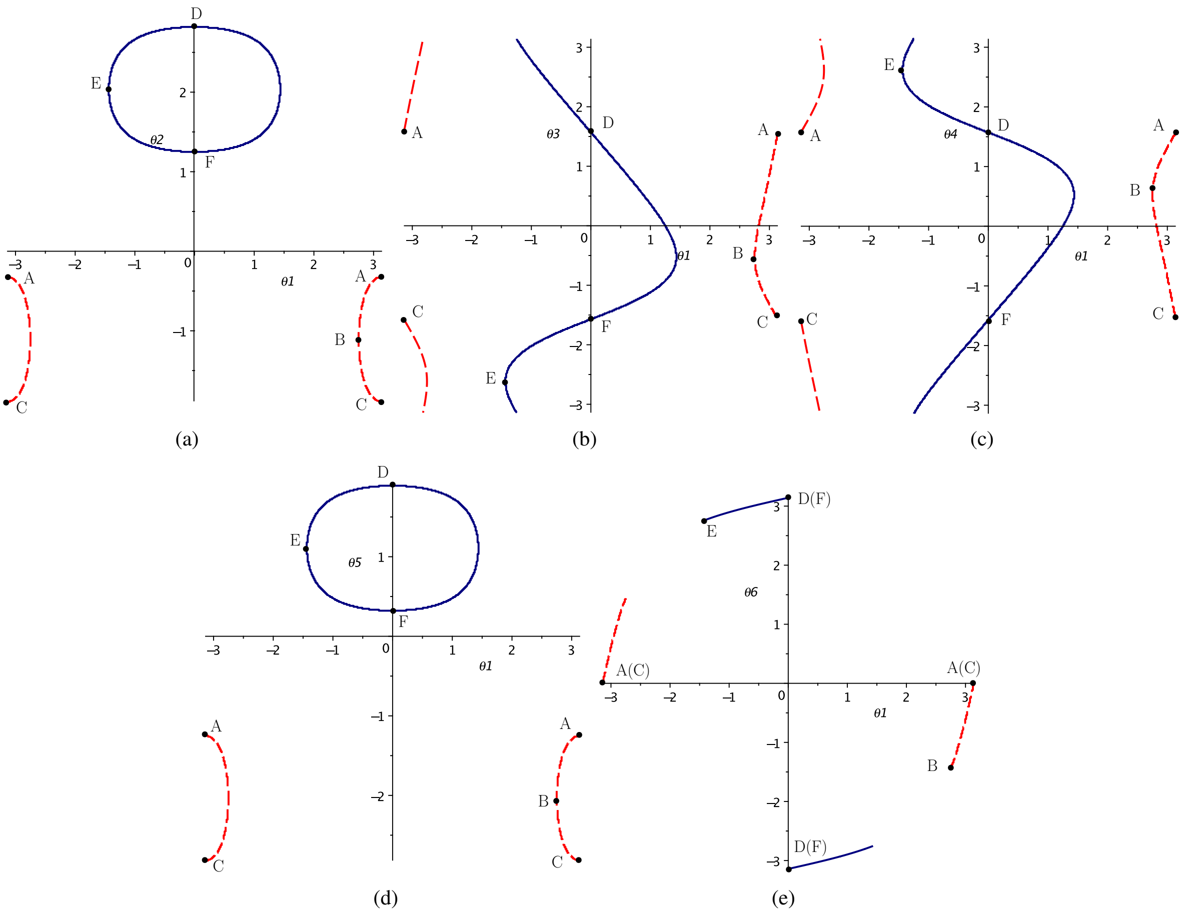

Fig. 6. Kinematic analysis of Mechanism I: (a) Plot of θ_1-θ_2, (b) Plot of θ_1-θ_3, (c) Plot of θ_1-θ_4, (d) Plot of θ_1-θ_5, (e) Plot of θ_1-θ_6.

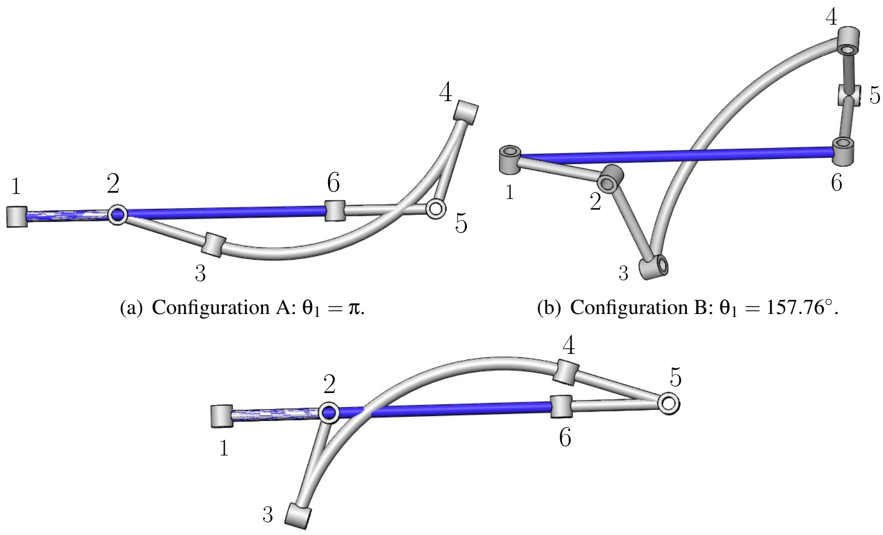

(a) Configuration A: $\theta_1 = \pi$. (b) Configuration B: $\theta_1 = 157.76°$.

(c) Configuration C: $\theta_1 = \pi$.

Fig. 7. Configurations of Mechanism I in Mode 1.

3.2 Mechanism II: Mechanism with two pairs of full-turn R joints

The link parameters of Mechanism II are:
$d_2 = d_5 = 0$, $d_6 = -d_1 = 0$, $d_4 = -d_3 = 50$,
$\alpha_1 = \alpha_2 = \alpha_4 = \alpha_5 = \pi/2$, $\alpha_6 = 0$, $\alpha_3 = \pi/2$,
$l_3 = 0$, $l_1 = l_2 = l_4 = l_5 = 120$, and $l_6 = 130\sqrt{2}$.

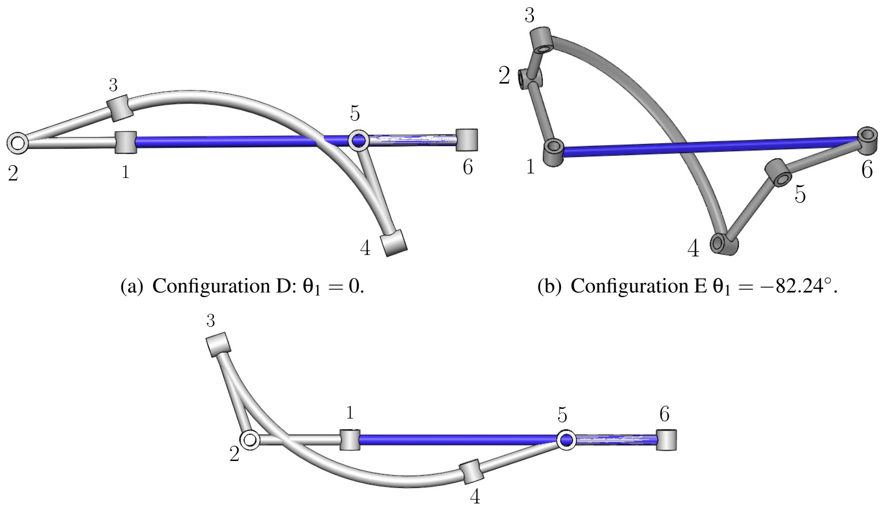

(a) Configuration D: $\theta_1 = 0$.

(b) Configuration E $\theta_1 = -82.24°$.

(c) Configuration F: $\theta_1 = 0$.

Fig. 8. Configurations of Mechanism I in Mode 2.

As in the case of Mechanism I detailed in Section 3.1, the input-output equation of Mechanism II is derived as

$$
\begin{aligned}
14161t_1^2t_2^2 + (15470\sqrt{2} - 28560)t_1^2t_2 + (37128\sqrt{2} - 54383)t_1^2 + (-285168\sqrt{2} + 403537)t_2^2 \\
+(134290\sqrt{2} - 190800)t_2 + 37128\sqrt{2} - 54383 = 0
\end{aligned}
\tag{36}
$$

Substituting $t_i = (1 + C\theta_i)/S\theta_i$ $(i = 1,2)$ into Eq.(36) and simplifying the resulted equation, we obtain

$$
\begin{aligned}
312C\theta_1C\theta_2 - 130C\theta_1S\theta_2 + 288\sqrt{2}C\theta_2 \\
-120\sqrt{2}S\theta_2 + 312C\theta_1 + 169\sqrt{2} = 0
\end{aligned}
\tag{37}
$$

For a given set of θ_1 and θ_2, one can determine θ_i by calculating $t_i = cot(\theta_i/2)$ using the following equations.

$$
\begin{aligned}
t_3 = (312\sqrt{2}t_1t_2^2 - 130\sqrt{2}t_1t_2 + 457t_1t_2^2 - 240t_1t_2 \\
-119t_1 - 338t_2)/(119t_2^2 - 240t_2 - 119)
\end{aligned}
\tag{38}
$$

$$
t_4 = (5t_3 + 12)/(12t_3 + 5) \tag{39}
$$

$$
t_5 = -(5t_2 + 12)/(12t_2 - 5) \tag{40}
$$

$$
t_6 = -(1/119)(312\sqrt{2} - 457)/t_1 \tag{41}
$$

The variation of θ_2 with respect to θ_1 for Mechanism II is shown in Fig. 9. It is observed that Mechanism II has two circuits shown in solid and dashed lines respectively and joints 1, 3, 4 and 6 are full-turn R joints. Figures 10 and 11 show Mechanism II at configurations A, B and C in circuit 1 and configurations D, E and F in circuit 2 respectively. Like Mechanism I, at two configurations in each circuit (see configurations A and C in circuit 1 and configurations D and F in circuit 2), the axes of R joints 1, 3, 4 and 6 of Mechanism II are coplanar and the axes of R joints 2 and 5 are perpendicular to the plane defined by the axes of R joints 1, 3, 4 and 6.

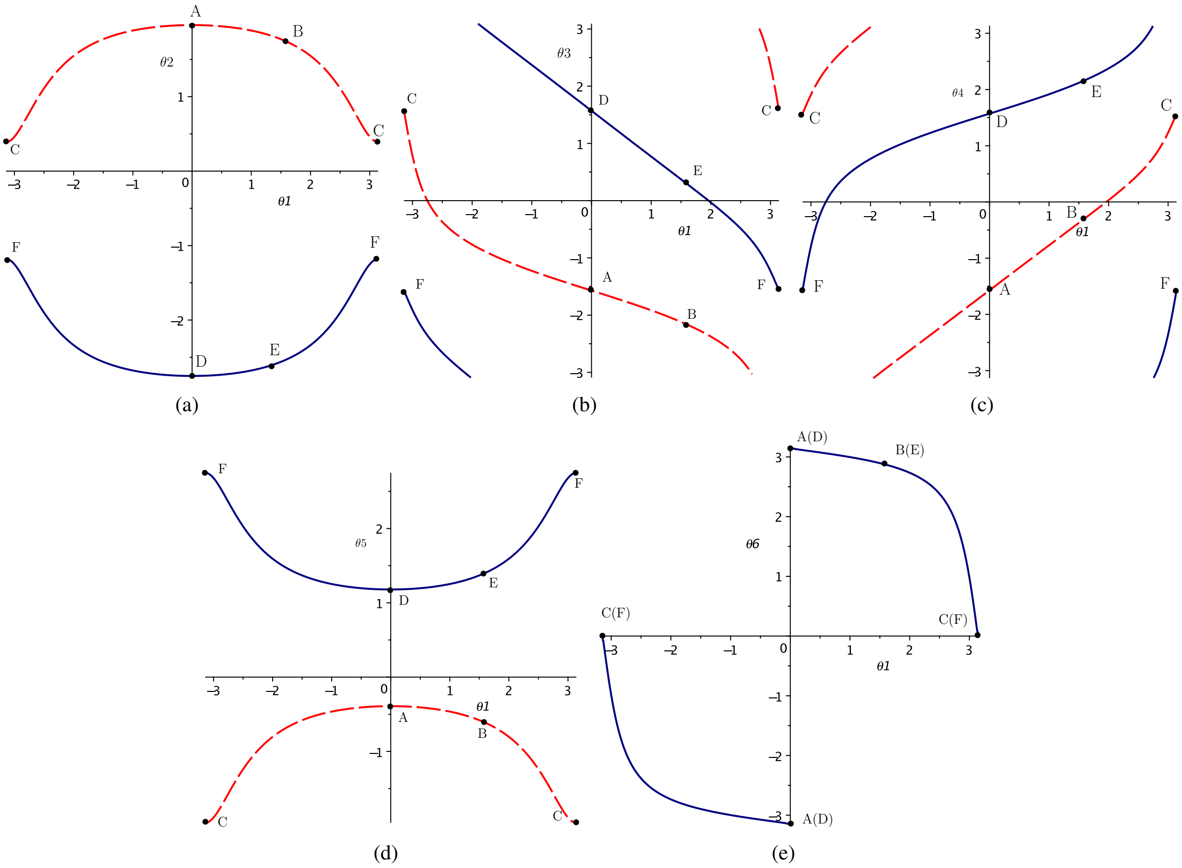

Fig. 9. Kinematic analysis of Mechanism II: (a) Plot of θ_1-θ_2, (b) Plot of θ_1-θ_3, (c) Plot of θ_1-θ_4, (d) Plot of θ_1-θ_5, (e) Plot of θ_1-θ_6.

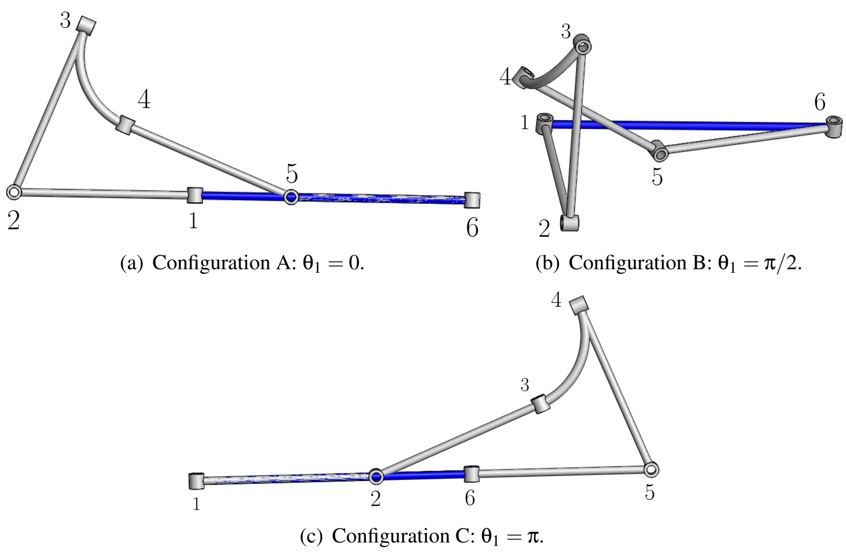

Fig. 10. Configurations of Mechanism II in Mode 1.

In addition, the explicit input-output equations between θ_3 (θ_4 or θ_5) and θ_1 are

$$\begin{aligned}&119t_1^2t_3^2+(130\sqrt{2}-240)t_1t_3^2-119t_1^2+(624\sqrt{2}-1152)t_1t_3\\&+(312\sqrt{2}-457)t_3^2+(130\sqrt{2}-240)t_1-312\sqrt{2}+457=0\end{aligned} \tag{42}$$

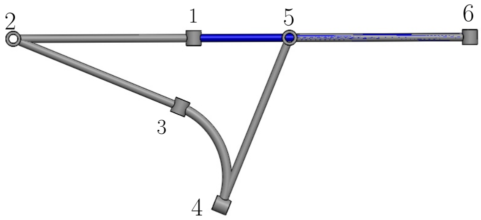

(a) Configuration D: $\theta_1 = 0$.

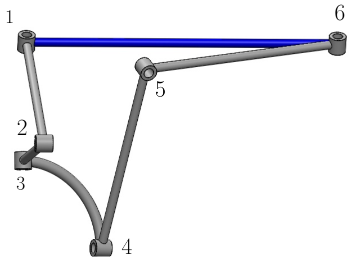

(b) Configuration E: $\theta_1 = \pi/2$.

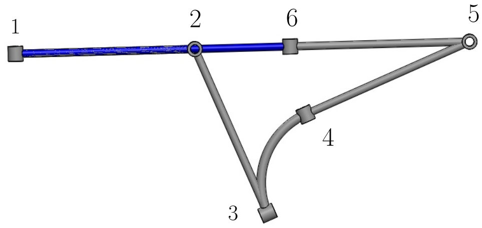

(c) Configuration F: $\theta_1 = \pi$.

Fig. 11. Configurations of Mechanism II in Mode 2.

$$
\begin{aligned}
&119t_1^2t_4^2 + (130\sqrt{2} - 240)t_1t_4^2 - 119t_1^2 + (-624\sqrt{2} + 1152)t_1t_4 \\
&\quad +(312\sqrt{2} - 457)t_4^2 + (130\sqrt{2} - 240)t_1 - 312\sqrt{2} + 457 = 0
\end{aligned}
\tag{43}
$$

$$
\begin{aligned}
&119t_1^2t_5^2 + (130\sqrt{2} + 240)t_1^2t_5 + (-312\sqrt{2} - 457)t_1^2 + 119t_5^2 \\
&\quad +(-130\sqrt{2} + 240)t_5 + 312\sqrt{2} - 457 = 0
\end{aligned}
\tag{44}
$$

4 Discussion

From the construction and kinematic analysis of the 6R mechanism, one can observe that from one configuration [Figs. 7(a), 10(a) and 11(a)] of the 6R mechanism, one can obtain another configuration [Figs. 8(c), 10(c) and 11(c)], called a shadow configuration, of the mechanism by simply renumbering the joints from 1, 2, $\cdots$, 6 to 6, 5, $\cdots$, 1. Such mechanisms are called two-faced mechanisms. In other words, the configurations of the mechanism appear in pairs and each pair of configurations are identical after renumbering the joints. It is noted that a configuration and its shadow configuration may be in the same circuit [Figs. 7(a) and 8(c)] or different circuits [Figs. 10(a) and 10(c); Figs. 11(a) and 11(c)].

As pointed out in section 2.3.3, this 6R mechanism can also be derived by merging two plane symmetric Goldberg-5R mechanisms [Fig. 5(b)]. Although a plane symmetric Goldberg-5R mechanism can reach a plane symmetric configuration, only the 6R mechanisms with two pairs of full-turn R joints can reach a plane symmetric configuration, while the 6R mechanisms with one pair of full-turn R joints cannot.

The above results have been verified using several mechanism models built using 3D printing. Figure 12 shows the CAD model and 3D-printed prototype of 6R Mechanism II in the configuration shown in Fig. 10(c). It is noted that joints 1 and 6 in this prototype are prevented from full-turn rotation due to interference between links 2 and 4 as well as links 1 and 5.

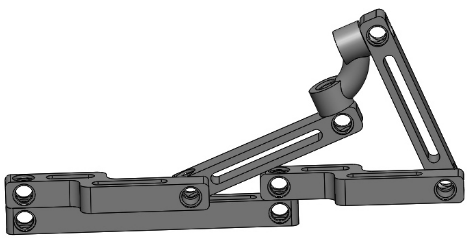

(a) CAD model.

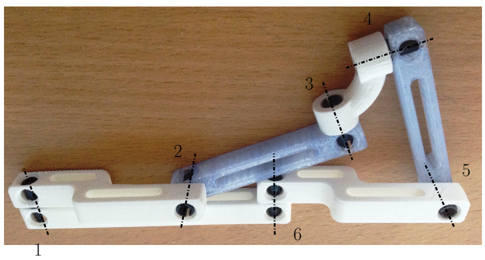

(b) 3D-printed prototype.

Fig. 12. A prototype of 6R Mechanism II.

It can be proved geometrically or algebraically that the axes of R joints 2 and 5 generally intersect with each other. Therefore, the proposed 6R mechanism has two pairs of R joints with intersecting axes (3 and 4; 2 and 5) and one pair of R joints with parallel axes (1 and 6). Unlike the Schatz's 6R mechanism, it has one link with intersecting joint axes. In addition, the proposed 6R mechanism can also be regarded as a variation of the 6R mechanism that has three pairs of R joints with intersecting axes [26]. It is noted that the overconstrained 6R mechanism detailed in [26] is also a double-faced mechanism.

Like a double-crank planar four-bar mechanism, Mechanisms I and II can be used as double-crank mechanisms if link 3 is selected as the frame, while Mechanism II can also be used as a double-crank mechanism if link 6 selected as the frame. The observation that joints 3 and 4 are always full-turn R joints is to be proved. Conditions under which joints 1 and 6 become full-turn R joints are still to be identified.

Unlike the mechanisms with certain symmetric characteristics, such as those in [42–44], that are symmetric in any single configuration of the mechanisms, the double-faced mechanism is usually not symmetric at a single configuration of the mechanism.

5 Conclusions

A 6R mechanism that has two pairs of R joints with intersecting axes and one pair of R joints with parallel axes has been constructed from an isosceles triangle and a pair of identical circles. The kinematic analysis using a dual quaternion based approach has shown that the 6R mechanism usually has two solutions to the kinematic analysis for a given input and this type of mechanisms may have two circuits (or closure modes) with one or two pairs of full-turn R joints. In two configurations in each circuit of the 6R mechanism, the axes of four R joints are coplanar, and the axes of the other two R joints are perpendicular to the plane defined by the above four R joints. From one configuration of the 6R mechanism, one can obtain another configuration of the mechanism by simply renumbering the joints. The concept of two-faced mechanism has been introduced.

This work enriches the geometric approach for identifying 6R overconstrained mechanisms. The formulas for the analysis of plane symmetric spatial triangle will also be useful for the design and analysis of multi-loop overconstrained mechanisms involving plane symmetric spatial RRR triads [45].

Acknowledgments

The authors would like to thank the Engineering and Physical Sciences Research Council (EPSRC), United Kingdom, for the support under grant No. EP/K031643/1. The work was also supported by the National Natural Science Foundation of China under grant No. 51375058 and 51775052 and Beijing Key Laboratory of Space-ground Interconnection and Convergence.

References

[1] Bricard, R., 1897, "Mémoire sur la théorie de l'octaèdre articulé," *Journal de Mathématiques Pures et Appliquées*, **3**: 113–148.
[2] Bricard, R., 1927, Lecons de cinématique. In: *Tome II Cinématique Appliquée*, pp. 7–12. Gauthier-Villars, Paris.
[3] Goldberg, M., 1943, "New five-bar and six-bar linkages in three dimensions," *Transactions of ASME*, **65**: 649–663.
[4] Waldron, K.J. 1968, "Hybrid overconstrained linkages," *Journal of Mechanisms*, **2**: 73–78.
[5] Wohlhart, K., 1987, "A new 6R space mechanism," In: *Proceedings of the 7th World Congress on Theory of Machines and Mechanisms*, Seville, Spain, 17–22 September 1987, vol. 1, pp. 193–198.
[6] Wohlhart, K., 1991, "Merging two general Goldberg 5R linkages to obtain a new 6R space mechanism," *Mech Mach Theory*, **26**(2): 659–668.
[7] Mavroidis, C., and Roth, B., 1995, "Analysis of overconstrained mechanisms," *J Mech Des-T ASME*, **117**: 69–74.
[8] Dietmaier, P., 1995, "A new 6R space mechanism," in: *Proceedings of the 9th World Congress IFToMM*, Milano, 1995, Vol. 1, pp. 52–56.
[9] Six, K., and Kecskeméthy, A., 1999, "Steering properties of a combined wheeled and legged striding excavator," *Proceedings of the 10th World Congress on the Theory of Machines and Mechanisms*, Oulu, Finland, June 20-24, 1999, vol. 1, pp. 135-140.
[10] Zsombor-Murray, P.J., and Gfrerrer, A., 2002, "'Robotrac' mobile 6R closed chain," *Proceedings of CSME Forum 2002*, ISBN 0-9730900, Kingston, Canada, May 21-24, 2002, Paper number, 02-05
[11] Baker, J.E., 2005, "A curious new family of overconstrained six-bars," *J Mech Des-T ASME*, **127**(4): 602–606.
[12] Baker, J.E., 2006, "On generating a class of foldable six-bar spatial linkages," *J Mech Des-T ASME*, **128**(2): 374–383.
[13] Chen, Y., and You, Z., 2007, "Spatial 6R linkages based on the combination of two Goldberg 5R linkages," *Mech Mach Theory*, **42**: 1484–1498.

[14] Baker, J.E., 2009, "Screw replacements in isomeric variants of Bricard's line-symmetric six-bar," *P I Mech Eng C-J Mec*, **223**(10): 2391–2398.

[15] Pfurner, M., 2009, "A new family of overconstrained 6R-mechanisms," *Proceedings of EUCOMES 08*, M. Ceccarelli (Ed), Springer Netherlands, 2009, pp. 117–124.

[16] Hegedüs, G., Schicho, J., and Schröcker, H.P. 2012, "Construction of overconstrained linkages by factorization of rational motions." *Latest Advances in Robot Kinematics*, J. Lenarčič, M. Husty (Eds.), Springer Netherlands, 2012, pp. 213-220.

[17] Chen, Y., and You, Z. 2012, "Spatial Overconstrained Linkages—The Lost Jade." *Explorations in the History of Machines and Mechanisms: Proceedings of HMM2012*, T. Koetsier, and M. Ceccarelli (Eds.), Springer Netherlands, Dordrecht, 2012, pp. 535–550.

[18] Li, Z., and Schicho, J., 2013, "Classification of angle-symmetric 6R linkages," *Mech Mach Theory*, **70**: 372–379.

[19] Li, Z., and Schicho, J., 2014, "Three types of parallel 6R linkages," *Computational Kinematics*, F. Thomas A. and Perez Gracia (Eds), Springer Netherlands, 2014, pp. 111–119.

[20] Li, Z., 2014, "Sharp Linkages," *Advances in Robot Kinematics*, J. Lenarcic, O. Khatib (Eds), Springer Netherlands, 2014, pp. 131–138.

[21] Hegedsa, G., Li, Z., Schichoc, J., Schröckerd, H.P., 2015, The theory of bonds II: Closed 6R linkages with maximal genus. *J Symb Comput*, **68**(2): 167–180.

[22] Kong, X., 2014, "Type synthesis of single-loop overconstrained 6R mechanisms for circular translation," J Mech Robot, **6**(4): 041016.

[23] Lee, C.C., and Hervé, J.M., 2014, "Geometric derivation of 6R linkages with circular translation," *Advances in Robot Kinematics*, J. Lenarčič and O. Khatib (Eds), Springer, Netherlands, 2014, pp. 59–67.

[24] Yarullin, M.G., Mingazov, M.R., and Galiullin, I.A., 2015, "Historical review of studies of spatial nR linkages," *Proceedings of 2015 IFToMM Workshop on History of Mechanism and Machine Science*, May 26–28, 2015, St-Petersburg, Russia.

[25] Li, Z., and Schicho, J., 2015, "A technique for deriving equational conditions on the Denavit-Hartenberg parameters of 6R linkages that are necessary for movability," *Mech Mach Theory*, **94**, pp. 1–8.

[26] Kong, X., 2016, "Geometric construction and kinematic analysis of a 6R single-loop overconstrained spatial mechanism that has three pairs of revolute joints with intersecting joint axes," *Mech Mach Theory*, **102**: 196–202.

[27] Kong, X., and Gosselin, C.M., 2004, "Type synthesis of three-degree-of-freedom spherical parallel manipulators," *Int J Robot Res*, **23**(3): 237–245.

[28] Kong, X., and Gosselin, C., 2007, *Type Synthesis of Parallel Mechanisms*, Springer, New York.

[29] Li, B., Huang, H., Deng, Z., 2015, "Mobility analysis of symmetric deployable mechanisms involved in a coplanar 2-twist screw system," *J Mech Robot*, **8**(1): 011007.

[30] Liu, C., Yao, S., Wang, H., and Yao, Y., 2015, "Ground mobile Schatz mechanism," *J Mech Robot*, **8**(1): 015002.

[31] Kong, X., and Huang, C., 2009, "Type synthesis of single-DOF single-loop mechanisms with two operation modes," *Proceedings of the 2009 ASME/IFToMM International Conference on Reconfigurable Mechanisms and Robots*, London, UK, 2009, pp. 136–141.

[32] Wohlhart, K., 2010, "Multifunctional 7R linkages," *Proceedings of the International Symposium on Mechanisms and Machine Theory*, AzCIFToMM, Izmir, Turkey, 2010, pp. 85–91.

[33] Song, C.Y.. Chen, Y., and Chen, I-M., 2013, "A 6R linkage reconfigurable between the line-symmetric Bricard linkage and the Bennett linkage," *Mech Mach Theory*, **70**: 278–292.

[34] He, X., Kong, X., Hao, G., and Ritchie, J., 2016, "Design and analysis of a new 7R Single-Loop mechanism with 4R, 6R and 7R operation modes," In *Advances in Reconfigurable Mechanisms and Robots II*. pp. 27–37. Springer International Publishing.

[35] Zhang, K., Müller, A., and Dai, J.S., 2016, "A novel reconfigurable 7R linkage with multifurcation." In *Advances in Reconfigurable Mechanisms and Robots II*. pp. 15–25. Springer International Publishing.

[36] Lpez-Custodio, P.C., Rico, J.M., and Cervantes-Snchez, J.J., Prez-Soto, G.I., 2016, "Reconfigurable mechanisms from the intersection of surfaces," *J Mech Robot*, 2016; **8**(2):021029-.

[37] Kong, X., 2016, "Kinematic analysis of conventional and multi-mode spatial mechanisms using dual quaternions," In *ASME 2016 International Design Engineering Technical Conferences and Computers and Information in Engineering Conference*. (Vol. 5B), DETC2016-59194, American Society of Mechanical Engineers.

[38] Racila, L., and Dahan, M., 2010, "Spatial properties of Wohlhart symmetric mechanism," *Meccanica*, **45**: 153–165.

[39] Lee, C.C., and Yan, H.S., 1993, "Movable spatial 6R mechanisms with three adjacent parallel axes," *J Mech Des-T ASME*, **115**(3): pp. 522–529.

[40] Kong, X. 2017, "Standing on the shoulders of giants: A brief note from the perspective of kinematics," *Chin J Mech Eng*, **30**(1): 1–2.

[41] Mavroidis, C. and Roth, B., 1996, "On the geometry of spatial polygons and screw polygons," *J Mech Des-T ASME*, **119**(1): 246–252.

[42] Selig, J.M., and Husty, M., 2011, “Half-turns and line symmetric motions,” *Mechanism and Machine Theory*, **46**(2): pp. 156–167.
[43] Kong, X., Yu, J., 2015, “Type synthesis of two-degrees-of-freedom 3-4R parallel mechanisms with both spherical translation mode and sphere-on-sphere rolling mode,” *ASME J. Mechanisms Robotics*, **7**(4): 041018.
[44] Wu, Y., Löwe, H., Carricato, M., and Li, Z., 2016, “Inversion symmetry of the Euclidean group: Theory and application to robot kinematics,” IEEE Transactions on Robotics, **32**(2): pp. 1–15.
[45] Wang, J. and Kong, X., 2017, “Deployable mechanisms constructed by connecting orthogonal Bricard linkages, 8R or 10R single-loop linkages using S joints ,” *Mech Mach Theory*, in press (DOI: 10.1016/j.mechmachtheory.2017.09.017).

